10

Optical spectroscopy of the Er^{3+} ions in $BaY_{1,8}Lu_{0,2}F_8$ crystals

© A.V. Astrakhantseva[1], A.A. Shavelev[1], S.V. Kuznetsov[2], A.G. Nikolaev[3], K.N. Boldyrev[4], A.S. Nizamutdinov[1], V.V. Semashko[1,5]

[1] Kazan Federal University, Kazan, Tatarstan, Russia
[2] Prokhorov Institute of General Physics, Russian Academy of Sciences, Moscow, Russia
[3] Institute of Geology and Oil and Gas Technologies, Kazan Federal University, 420008 Kazan, Russia
[4] Institute of Spectroscopy, Russian Academy of Sciences, Troitsk, Moscow, Russia
[5] the Zavoisky Physical-Technical Institute, FRC Kazan Scientific Center of RAS, 420029 Kazan, Russia

e-mail: anya4324@gmail.com

Received November 01, 2022
Revised April 10, 2023
Accepted April 11, 2023

The spectral and kinetic characteristics of Er^{3+} ions in heavily doped $BaY_{1.8}Lu_{0.2}F_8$ mixed crystals have been studied. Absorption and luminescence spectra were recorded for $BaY_{1.8}Lu_{0.2}F_8$ crystals with Er^{3+} ion concentrations of 20.0 and 30.0 at.%. The kinetic dependences of luminescence decay in the infrared range have also been studied. A model of the level populations of Er^{3+} ions is constructed on the basis of a three-level scheme for pumping the $^4I_{11/2}$ state at a wavelength of 970 nm without taking into account up-conversion processes. The gain of $BaY_{1.8}Lu_{0.2}F_8$ crystals with Er^{3+} ion concentrations of 20.0 and 30.0 at.% is estimated at different pump powers.

Keywords: population inversion, gain coefficient, modeling, fluorides.

DOI: 10.61011/EOS.2023.05.56504.61-22

Introduction

Erbium ions allow to achieve effective laser radiation in the wavelength range of about 1.5 and 2.7 μm [1,2]. In turn, lasers emitting in the infrared range are the basis for the creation of laser gas analyzers used in differential optical absorption spectroscopy to determine greenhouse gases and water. The advantage of using fluorides as an active laser medium among other crystalline matrices is their transparency from ultraviolet (UV) to infrared (IR) spectral regions and low phonon energy, which leads to a long lifetime of electronic states due to a decrease in the probability of nonradiative transitions [3–5]. The inclusion of Lu^{3+} ions in the matrix cations and the growth of mixed $BaY_{1-x}Lu_xF_8$ crystals is considered as one of the ways to broaden the spectral lines of transitions [6]. According to the data [7], from the spectrum of the radiation cross section for the $BaY_2F_8:Ho^{3+}$ crystal, the width of the $^5I_7 \rightarrow {}^5I_8$ transition line can be evaluated at a level of 20% of the peak height, it was approximately 140.5 nm. At the same time, for a crystal with the addition of $Lu^{3+}BaY_{1-x}Lu_xF_8:Ho$ ions from the radiation spectrum in the paper [8], the linewidth of the same transition at a level of 20% of the peak height is evaluated to be approximately 177 nm.

An important characteristic of the active medium is the amplification band. Many applications require a wide amplification bandwidth, which allows for wavelength tunability or the generation of ultrashort laser pulses.

The purpose of this paper is to study the spectral and kinetic characteristics of $BaY_{1.8}Lu_{0.2}F_8$:Er mixed crystals doped with high concentrations of Er^{3+} ions and to model the amplification factor of this active medium in the IR spectral range without taking into account up-conversion processes.

Experimental part

Samples of $BaY_{1.8}Lu_{0.2}F_8$:Er crystals with Er^{3+}ion concentrations of 20 and 30 at.% were grown by the Bridgman method in vacuum in graphite crucibles and with a graphite resistive heater at the Department of Quantum Electronics and Radio Spectroscopy of the Institute of Physics, Kazan Federal University. The initial components were taken from commercially available sources and were 99.999% pure. The growth rate was 1.2 mm/hour. As a result, single crystals with a diameter of 8 mm and a length of 30 mm were grown. The disks were polished to a thickness of 2 mm (sample with Er^{3+} 20 at.% concentration) and 1 mm (sample with Er^{3+} 30 at.% concentration). A photograph of single-crystal disks is shown in Fig. 1.

Luminescence spectra in the wavelength range 850–2900 nm at room temperature were recorded on a wide-range IR Fourier spectrometer Bruker IFS125HR with a spectral resolution better than 0.2 nm, and laser excitation at a wavelength of 525 nm, the power density on the sample was 50 mW/cm^2. CaF_2 was used as

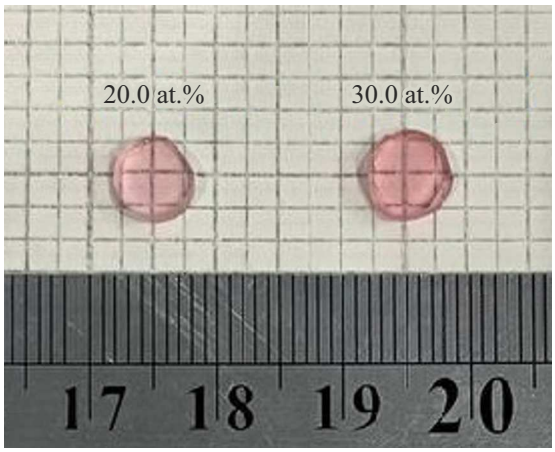

Figure 1. Photo of samples of $BaY_{1.8}Lu_{0.2}F_8$:Er crystals with Er^{3+} 20 and 30 at.% concentrations.

a beam splitter, and —nitrogen-cooled InSb as a detector. The recorded luminescence spectra were normalized to the spectral sensitivity of the instrument. To reduce the effect of reabsorption in the volume of the sample, the luminescence light was collected by a spherical mirror from the surface onto which the excitation beam was incident. Absorption spectra in the wavelength range 350−1650 nm were recorded at room temperature on a Shimadzu UV-3600 spectrophotometer. The measurements were carried out in non-polarized schemes, since the shape of the absorption spectra in the IR range does not change significantly for different orientation diagrams [9].

The luminescence kinetics were studied upon excitation by a laser diode at a wavelength of 970 nm using an MDR-23 monochromator, photomultiplier PMT-62 for the near-IR range and a detector based on a PD24 avalanche photodiode for the IR range served as photodetectors.

Absorption and luminescence spectra, luminescence kinetics

Based on the recorded absorption spectra of single-crystals $BaY_{1.8}Lu_{0.2}F_8$:Er with ion concentrations Er^{3+} 20 and 30 at.%, the values of the absorption cross section (Fig. 2) were calculated using the formula

$$\sigma_{abs} = \alpha_{abs}/N_{Er}. \quad (1)$$

Here N_{Er} — Er^{3+} ion concentration, α_{abs} — absorption coefficient. The absorption spectra of Er^{3+} ions in the samples are due to transitions from the ground state $^4I_{15/2}$ to excited states $^4G_{7/2}$, $^4G_{9/2}$, $^4G_{11/2}$, $^2H_{9/2}$, $^4F_{5/2}$, $^4F_{7/2}$, $^2H_{11/2}$, $^4S_{3/2}$, $^4F_{9/2}$, $^4I_{9/2}$, $^4I_{11/2}$,$^4I_{13/2}$ and correspond to literature data [10, 11]. The spectra form did not differ in the localization of the spectral lines, the number of peaks, and the nature of the broadening with an increase in the content of Er^{3+}, but had some changes that determine the difference in the transition probabilities. The latter may be due to

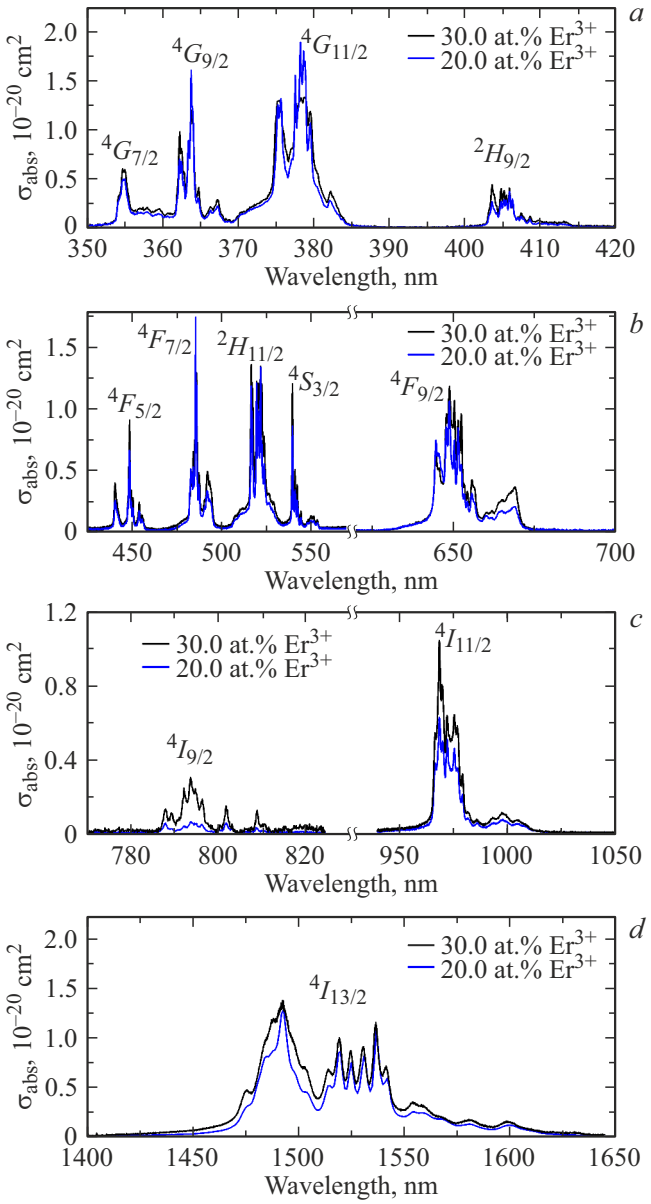

Figure 2. Absorption cross section spectra of $BaY_{1.8}Lu_{0.2}F_8$:Er crystals with concentrations of 20.0 and 30.0 at.%.

differences in the local structure of the crystal field near the impurity center Er^{3+}, to which the distribution of Lu^{3+} ions in the crystal lattice can also contribute. This requires further research for a series of crystals with different Y:Lu ratios.

Luminescence kinetics of $BaY_{1.8}Lu_{0.2}F_8$ crystals with Er^{3+}ion concentrations 1, 5, 10 , 20, and 30 at.% were recorded at a wavelength of 1000 nm ($^4I_{11/2} \rightarrow {}^4I_{15/2}$) and 1598 nm ($^4I_{13/2} \rightarrow {}^4I_{15/2}$) upon excitation at a wavelength of 970 nm at room temperature (Fig. 3, 4).

The luminescence decay curves were approximated by a single-exponential law; the decay time for the $^4I_{11/2}$ state was 5.68 ± 0.07 and 5.0 ± 0.2 ms for 20 and 30 at.% Er^{3+}, respectively. For the $^4I_{13/2}$ state, the luminescence decay

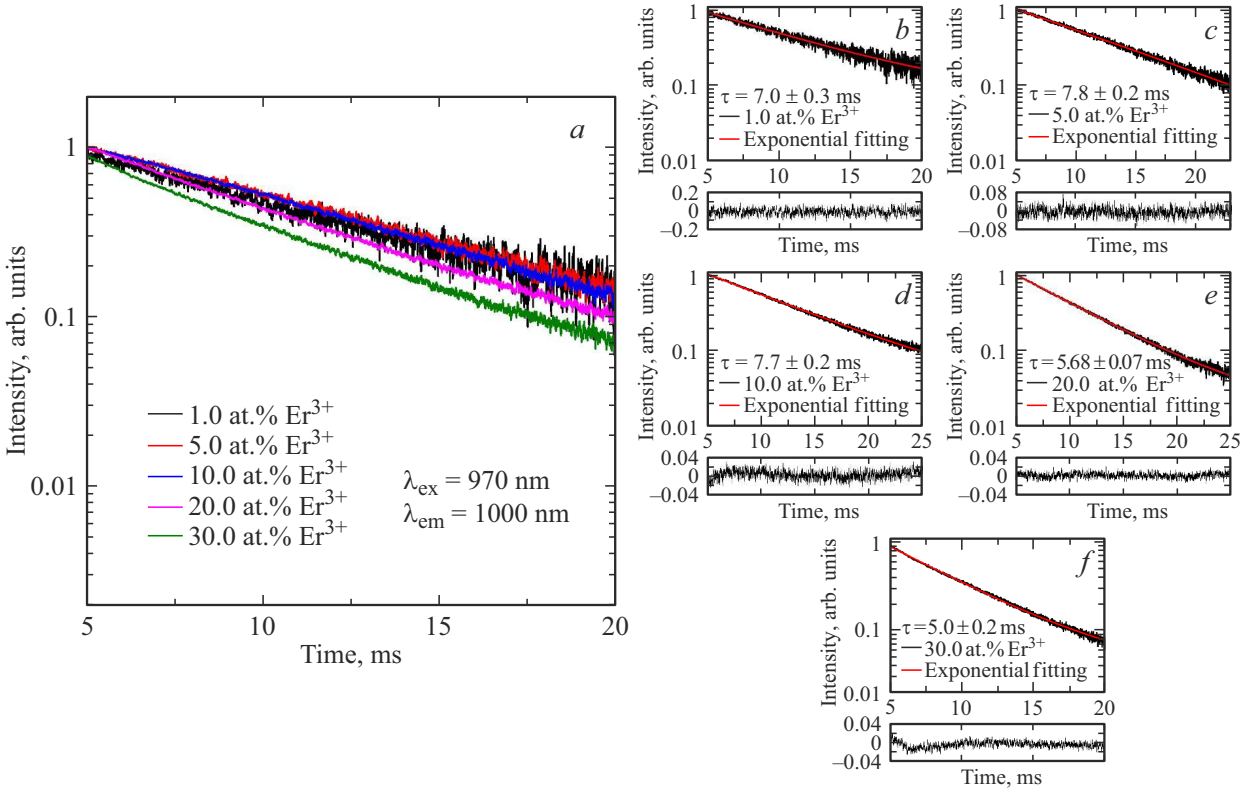

Figure 3. Luminescence kinetics of the state $^4I_{11/2}$, $\lambda_{ex} = 970$ nm, $\lambda_{em} = 1000$ nm for (*a*) all samples $BaY_{1.8}Lu_{0.2}F_8$:Er; (*b-f*) 1, 5, 10, 20 and 30 at.% Er^{3+} in $BaY_{1.8}Lu_{0.2}F_8$:Er crystals. The inserts show the corresponding residual functions.

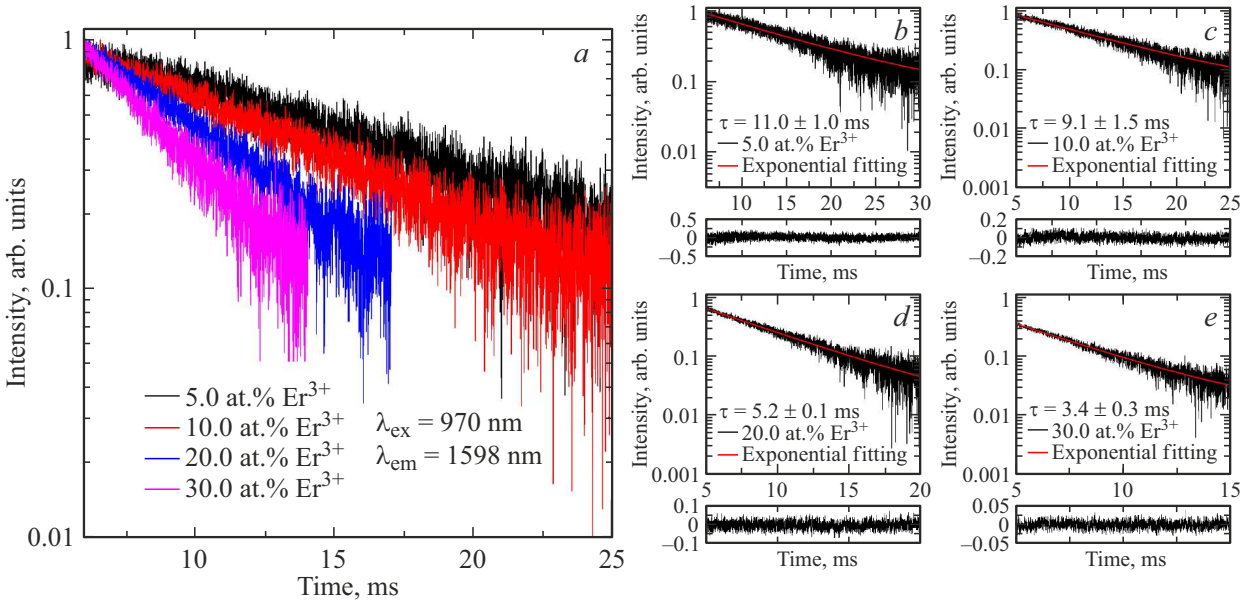

Figure 4. Luminescence kinetics of the state $^4I_{13/2}$, $\lambda_{ex} = 970$ nm, $\lambda_{em} = 1598$ nm for (*a*) all samples $BaY_{1.8}Lu_{0.2}F_8$:Er; (*b-f*) 1, 5, 10, 20 and 30 at.% Er^{3+} in $BaY_{1.8}Lu_{0.2}F_8$:Er crystals. The inserts show the corresponding residual functions.

time is 5.2 ± 0.1 and 3.4 ± 0.3 ms for Er^{3+} ion concentrations of 20 and 30 at.%, respectively. With an increase in the concentration of Er^{3+} ions in $BaY_{1.8}Lu_{0.2}F_8$:Er samples, there is concentration quenching. It is important that the lifetime of the $^4I_{11/2}$ state, which is the upper laser state for generation of approximately 2.7 μm, turns out to be longer than the lifetime of the $^4I_{13/2}$ state, which is the lower laser state.

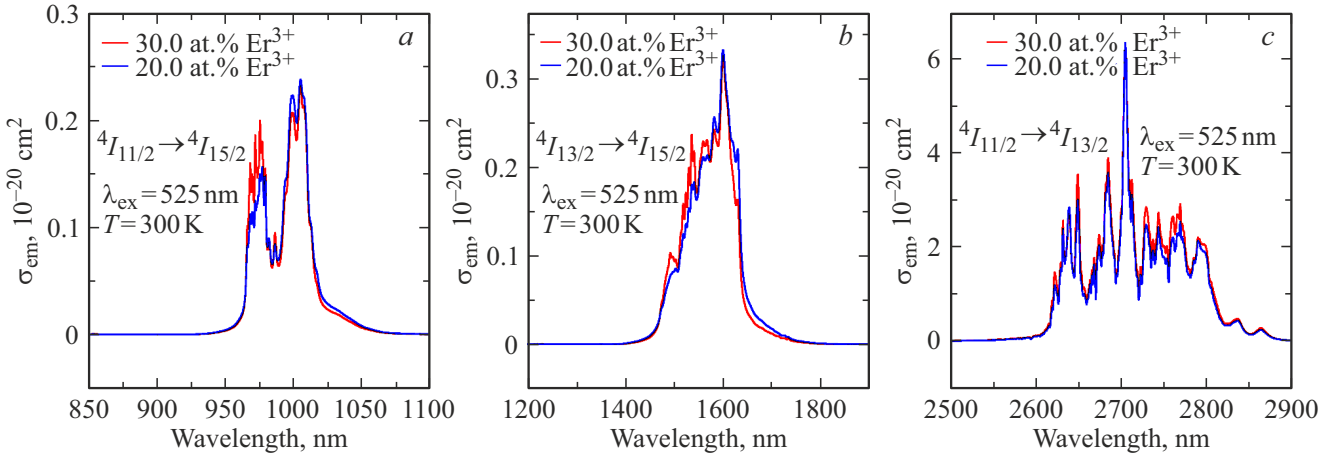

Figure 5. Stimulated emission cross section spectra of $BaY_{1.8}Lu_{0.2}F_8$:Er crystals with Er^{3+} concentrations of 20 and 30 at.%.

The stimulated emission cross sections were estimated for the ${}^4I_{11/2} \rightarrow {}^4I_{15/2}$, ${}^4I_{13/2} \rightarrow {}^4I_{15/2}$ and ${}^4I_{11/2} \rightarrow {}^4I_{13/2}$ transitions from the luminescence spectrum using the Fuchtbauer–Ladenburg formula [1,12]:

$$\sigma_{\text{em}}(\lambda) = \frac{\lambda^5}{8\pi n^2 \tau_{\text{rad}} c} \frac{W_{\text{em}}(\lambda)}{\int \lambda W_{\text{em}}(\lambda) d\lambda}. \qquad (2)$$

Here $W_{\text{em}}(\lambda)$ — luminescence intensity corrected for the sensitivity of the measuring system, τ_{rad} — radiative lifetime, n — refraction index of the sample, c — speed of light in vacuum.

The IR luminescence spectra of $BaY_{1.8}Lu_{0.2}F_8$ crystalline samples with Er^{3+} ion concentrations of 20 and 30 at.% were recorded at room temperature upon excitation at a wavelength of 525 nm. The radiative lifetime of τ_{rad} was calculated from experimental data on the luminescence decay kinetics in low-concentration $BaY_{1.8}Lu_{0.2}F_8$ samples with Er^{3+} ion concentration of 1 at.% at a wavelength of 1000 nm and 5 at.% at a wavelength of 1598 nm.

The unpolarized spectra of the stimulated emission cross section of the ${}^4I_{11/2} \rightarrow {}^4I_{15/2}$, ${}^4I_{13/2} \rightarrow {}^4I_{15/2}$ and ${}^4I_{11/2} \rightarrow {}^4I_{13/2}$ transitions for $BaY_{1.8}Lu_{0.2}F_8$: Er crystal samples with Er^{3+} 20 and 30 at.% concentrations are shown in Fig. 5. It can be seen from Fig. 5 that for the $BaY_{1.8}Lu_{0.2}F_8$:Er samples with Er^{3+} ion concentrations 20 and 30 at.%, the form of the lines of the spectrum of the stimulated emission cross section does not change significantly.

Amplification simulation

Let us review the three-level laser diagram shown in Fig. 6. The ${}^4I_{11/2}$ level is continuously pumped at a wavelength of 970 nm. Further, the population from the continuously pumped level ${}^4I_{11/2}$ relaxes to the ground state ${}^4I_{15/2}$ and with radiation to the lower laser level ${}^4I_{13/2}$

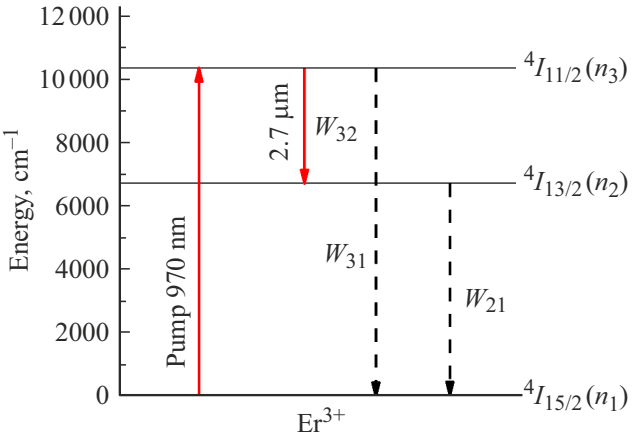

Figure 6. Energy diagram of Er^{3+} ion levels.

with the branching ratios β_{32}. The rate equations for the three-level diagram can be written as

$$\frac{dn_1}{dt} = -n_1\sigma_{13}I + \frac{n_2}{\tau_2} + \frac{n_3\beta_{31}}{\tau_3}, \qquad (3)$$

$$\frac{dn_2}{dt} = \frac{n_3\beta_{32}}{\tau_3} - \frac{n_2}{\tau_2}, \qquad (4)$$

$$\frac{dn_3}{dt} = n_1\sigma_{13}I - \frac{n_3\beta_{32}}{\tau_3} - \frac{n_3\beta_{31}}{\tau_3}, \qquad (5)$$

where n_i — number of ions per volume at the level i, σ_{13} — absorption cross section of the transition ${}^4I_{15/2} \rightarrow {}^4I_{11/2}$, I — pump intensity in $\text{cm}^{-1}\text{s}^{-1}$, β_{32} and β_{31} — luminescence branching factors, τ_i — lifetime level of i.

Using the experimentally obtained values of the lifetimes of the excited states of the Er^{3+} ion and the luminescence branching factors ($\beta_{32} = 0.23$, $\beta_{31} = 0.77$ for a sample with a concentration Er^{3+} of 20.0 at.% and $\beta_{32} = 0.15$, $\beta_{31} = 0.84$ for a sample with a concentration Er^{3+} of 30.0 at.%), the system of differential equations (3)–(5) was solved numerically, as a result of which the

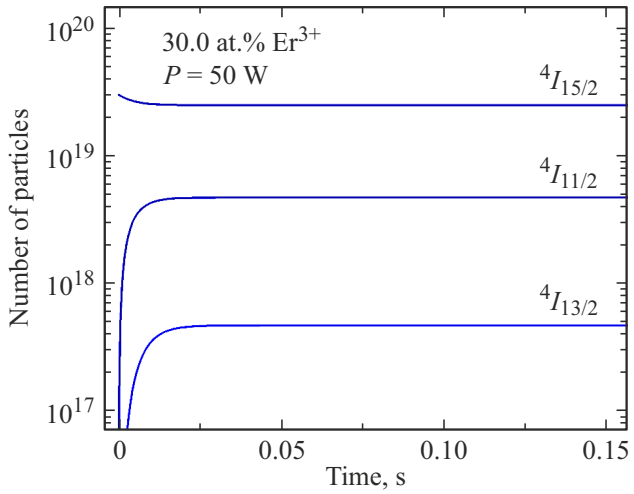

Figure 7. Population distribution of Er^{3+} ion levels (30.0 at.%) in the $BaY_{1.8}Lu_{0.2}F_8$ sample at a continuous pumping power of 50 W.

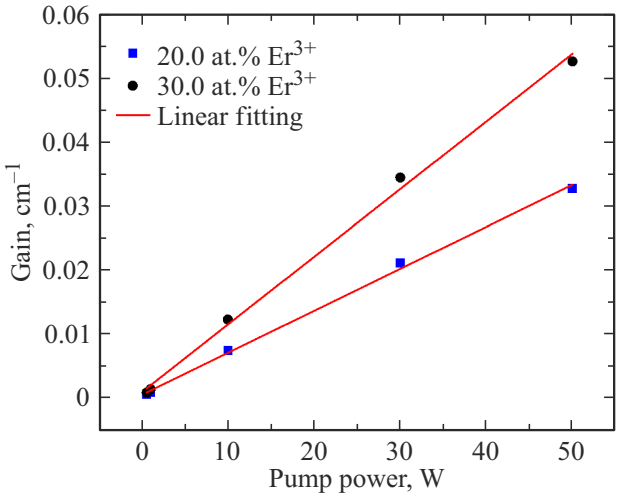

Figure 8. Dependence diagram of $BaY_{1.8}Lu_{0.2}F_8$:Er crystals amplification factor with Er^{3+} concentrations of 20.0 and 30.0 at.% as a function of the cw pumping power. Red lines — linear approximations.

population distributions over states were obtained. It is shown that between the states $^4I_{11/2}$ and $^4I_{13/2}$ under continuous pumping of different powers – from 550 mW to 50 W — a population inversion is achieved. Fig, 7 shows the level population distribution of the Er^{3+} ion for the $BaY_{1.8}Lu_{0.2}F_8$ sample with an active impurity concentration of 30.0 at.% under continuous pumping with a power of 50 W. It can be seen from Fig. 7 that a population inversion is achieved between the upper laser level $^4I_{11/2}$ and the lower laser level $^4I_{13/2}$ under continuous pumping.

This model was used to estimate the amplification of the active medium on $BaY_{1.8}Lu_{0.2}F_8$:Er crystals with Er^{3+} concentrations of 20 and 30 at.% (Fig. 8). Fig. 8 demonstrates the linear dependence of the amplification of the active medium on the pumping power. In this case, the sample with a Er^{3+} at.% concentration has a higher amplification compared to a sample with a Er^{3+} 20 at.% concentration.

Fig. 9 shows the amplification spectra calculated by solving the rate equations for $BaY_{1.8}Lu_{0.2}F_8$:Er samples with Er^{3+} concentrations of 20 and 30 at.% at different pumping powers. The inserts show the spectra at low powers — 1 W and 550 mW. It can be seen from Figs 9,*a* and 9,*b* that the form of the spectra does not change significantly for crystals with Er^{3+} ion concentrations of 20 and 30 at.%. Meanwhile, the spectra are saturated with lines of transitions between Stark states and potentially cause wavelength tuning in a wide range of approximately 2.7 μm.

Conclusion

In the present paper, the absorption and luminescence spectra were studied, as well as the luminescence decay kinetics in the IR area, of promising IR active media $BaY_{1.8}Lu_{0.2}F_8$ activated by Er^{3+} ions with concentrations from 1 to 30 at.%.

It is shown that for Er:$BaY_{1.8}Lu_{0.2}F_8$ crystals with a high concentration of Er^{3+} (more than 20 at.%) the lifetime of the $^4I_{13/2}$ state becomes shorter than the lifetime of the $^4I_{11/2}$ state; consequently, it is possible to achieve high lasing efficiency on these crystals at a wavelength of approximately 2.7 μm (transition $^4I_{11/2} \rightarrow {}^4I_{13/2}$). With the help of simulation of the populations on the laser states of the Er^{3+} ion for generation of approximately 2.7 μm, it was shown that between the states $^4I_{11/2}$ and $^4I_{13/2}$ with continuous pumping of different power — from 550 mW to 50 W — population inversion is achieved. The evaluation of the amplification factor based on the simulation results showed that the sample with the Er^{3+}30 at.% concentration has a higher amplification factor compared to the sample with the Er^{3+}20 at.% concentration. Meanwhile, the amplification spectra are saturated with lines of transitions between Stark states and potentially cause wavelength tuning in a wide range of approximately 2.7 μm, which makes the active medium promising for wavelength-tunable laser generation and shortening of the pulse duration.

Acknowledgments

Experiments to determine the characteristics of crystals were carried out at the expense of the FZSM-2022-0021 subsidy allocated to Kazan Federal University to implement the state assignment in the field of scientific activity.

Conflict of interest

The authors declare that they have no conflict of interest.

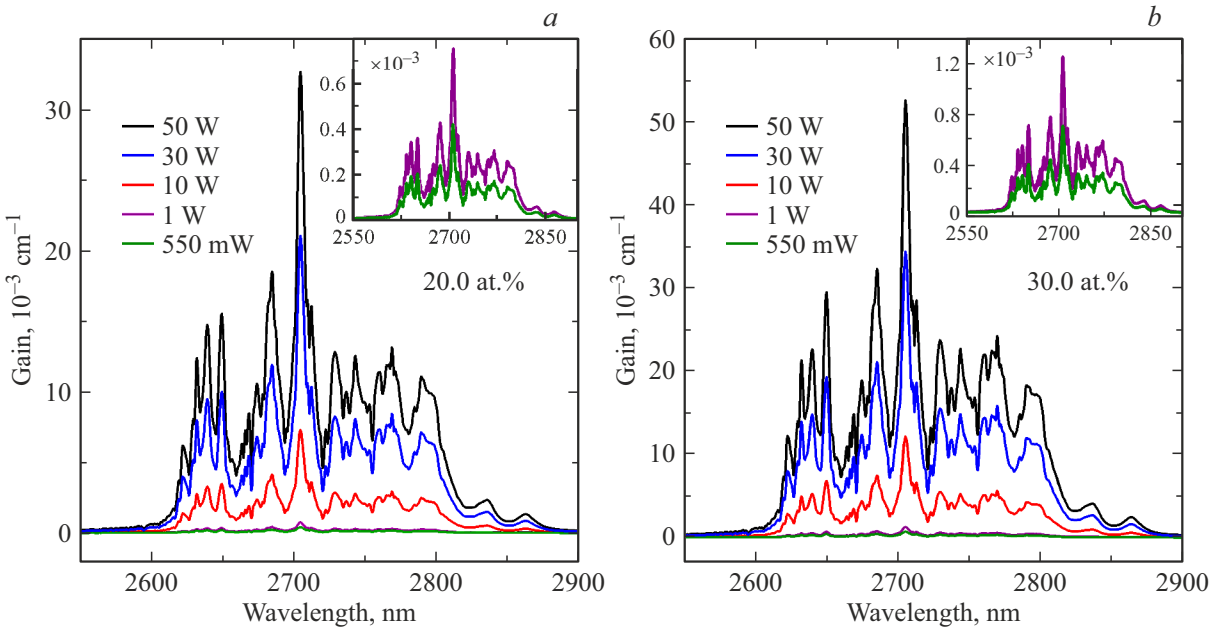

Figure 9. Amplification spectra of $BaY_{1.8}Lu_{0.2}F_8$:Er crystals with Er^{3+} concentrations: 20 (*a*), 30 at.% (*b*).

References

Translated by E.Potapova

[1] K.N. Gorbachenya, A.S. Yasukevich, V.E. Kisel, K.V. Lopukhin, V.V. Balashov, A.V. Fedin, M.N. Gerke, E.A. Volkova, V.O. Yapaskurt, N.N. Kuzmin, D.A. Ksenofontov, D.V. Korost, N.V. Kuleshov. Crystals, **12**(4), 519 (2022).

[2] K.N. Gorbachenya, S.V. Kurilchik, V.E. Kisel, A.S. Yasukevich, N.V. Kuleshov, A.S. Nizamutdinov, S.L. Korableva, V.V. Semashko. Quant. Electron., **46**(2), 95–99 (2016).

[3] A. Bitam, S. Khiari, M. Diaf, H. Boubekri, E. Boulma, C. Bensalem, L. Guerbous, J.P. Jouart. Opt. Mater., **82**, 104–109 (2018).

[4] S. Kuznetsov, Yu. Ermakova, V. Voronov, P. Fedorov, D. Busko, I.A. Howard, B.S. Richards, A. Turshatov. J. Mater. Chem. C, **6**(3), 598–604 (2018).

[5] E.I. Madirov, V.A. Konyushkin, A.N. Nakladov, P.P. Fedorov, T. Bergfeldt, D. Busko, I.A. Howard, B.S. Richards, S.V. Kuznetsov, A. Turshtov. J. Mater. Chem. C, **9**(10), 3493–3503 (2021).

[6] G. Turri, C. Gorman, A. Cassanho, M. Bass, H.P. Jenssen. JOSA B, **28**(2), 331–335 (2011).

[7] K.M. Dinndorf, H. Miller, A. Tabirian, H.P. Jenssen, A. Cassanho. *Advanced Solid State Lasers* (Optica Publishing Group, WB17, 1999).

[8] B.R. DeShano, G. Cook, T.R. Harris, H.P. Jenssen, A. Cassanho. SPIE, **10637**, 122–127 (2018).

[9] E. Sani, A. Toncelli, M. Tonelli. Opt. Mater., **28** (11), 1317–1320 (2006).

[10] S.A. Payne, L.L. Chase, L.K. Smith, W.L. Kway, W.F. Krupke. IEEE J. Quant. Electr., **28** (11), 2619–2630 (1992).

[11] A.A. Kaminskii, S.E. Sarkisov, F. Below, H.-J. Eichler. Opt. Quant. Electron., **22**, S95–S105 (1990).

[12] A.S. Yasyukevich, V.G. Shcherbitskii, V.É. Kisel', A.V. Mandrik, N.V. Kuleshov. J. Appl. Spectr., **71** (2), 202–208 (2004).